A new method for parameterization of wave dissipation by sea ice

Jie Yu, W. Erick Rogers and David W. Wang

Naval Research Laboratory, Stennis Space Center, MS 39529, USA

Key Points:

- A new method improves the prediction of wave dissipation, by using the dimensional analysis of data and an ice-thickness based scaling.
- A new wave dissipation model describes a nonlinear dependence on ice thickness and a condition of similarity between field and lab data.
- The prediction error is significantly reduced when applied to field data. The dissimilarity between field and lab data is resolved.

Corresponding author: Jie Yu, Jie.Yu@nrlssc.navy.mil

Abstract

We present a method for predicting wave dissipation by sea ice that is based on the dimensional analysis of data with a scaling defined by ice thickness. Applying the method to an extensive dataset from the measurements during the "Polynyas, Ice Production, and seasonal Evolution in the Ross Sea" (PIPERS) cruise in 2017, we derive a new model of wave dissipation which not only describes a nonlinear dependence on ice thickness but also reveals its relation with the dependence on frequency. This nonlinear dependence on ice thickness can have more implications on predicting low-frequency waves. The root-mean-square error of the prediction is significantly reduced using the new model, compared with other existing parametric models that are also calibrated for the PIPERS dataset. The new model also explicitly describes a condition of similarity between large- and small-scale observations, which is shown to exist when various laboratory datasets collapse onto the prediction.

Plain Language Summary The dissipation of wave energy by sea ice is physically complex due to waves interacting with various forms of ice, such as large sheet, floes, slushy ice-water mixture. Theories of wave-ice interaction are limited due to lack of appropriate mathematical representation of ice. In large-scale operational modeling, we generally use empirical formulas to parameterize the collective effects of ice. Clearly, the accuracy of such empirical models determines the accuracy of operational forecast/prediction of wave energy distribution in ice-infested oceans. We develop a new method to improve the parameterization of wave dissipation in sea ice, using an engineering tool of dimensional analysis with an ice-thickness based scaling. The scaling causes data to collapse towards a general trend, revealing the relations among physical variables. Applying the method to a large field dataset, we derive a new model of wave dissipation which describes a nonlinear dependence on ice thickness, and its relation to the dependence on frequency. It significantly reduces the error of prediction when compared with other parametric models that are also calibrated for the same dataset. When extrapolated, it agrees very well with various lab datasets, thus showing the condition of similarity between small-scale lab and field observations.

1 Introduction

As large-scale operational wave models have become relatively mature, e.g. WAVEWATCH III® (WW3) (Tolman, 1991; WW3DG, 2019) on the global domain and SWAN

('Simulating Waves Nearshore', Booij et al., 1999; SWAN team, 2019) on high-resolution coastal grids, a few frontier areas remain in which the models often struggle to perform well, and present new challenges (Rogers, 2020). One of them is the model dynamics for wave spectral distribution in ice-infested regions.

In the literature, theoretical studies often treat the ice-agglomeration layer as a continuum, invoking physical parameters which are practically not measurable, e.g., the effective viscosity and elasticity of broken ice, pancakes and frazil ice in marginal ice zones. Calibration of those effective properties is not trivial, due to the complex ice conditions and physics in wave-ice interaction. This makes theories difficult to apply. On the other hand, there are various laboratory and field studies, aiming to quantify wave dissipation by ice in a way that may be generalized. (We will not attempt a general review of the literature, since it will be unwise, in view of the size of published theoretical and experimental works. We shall restrict ourself to the references that are directly relevant to the purpose of this study.) During the past decade, the wave-ice community has recognized an apparent discrepancy between dissipation rates estimated from large-scale field studies versus small-scale laboratory studies. In the former, e.g., the Antarctic SIPEX-II data in Meylan et al. (2014) and Kohout et al. (2014), the Weddell Sea data in Doble et al. (2015), and the Arctic 'Sea State' data in Rogers et al. (2016) and Cheng et al. (2017), the wave-amplitude attenuation rates $k_i(1/\mathrm{m})$ are orders of magnitude smaller than those from lab studies such as Newyear & Martin (1997), Wang & Shen (2010), Zhao & Shen (2015), and Parra et al. (2020). Of course, they occupy different frequency ranges, but if any reasonable extrapolation is used, the apparent discrepancy is striking (Figure 1). Even within the similar scale, datasets from different studies are dissimilar, and the scattering of data is so large that a general trend cannot be derived with high confidence. The disconnect between data in different scales poses the questions: Are there different dissipation mechanisms in lab settings from the field? Are lab studies capable of informing wave-ice interaction in real oceans? But, through the history of science, we have built tremendous amount of knowledge in many disciplines based on controlled lab studies, such as turbulence.

Attempting to understand the differences and connections among various continuum-based theories on wave dispersion relationship (which describes the propagation and dissipation of linear waves) in ice-covered waters, Yu et al. (2019) applied dimensional analysis (an engineering tool to seek relationship among physical variables) to the existing

theories. By introducing a normalization (scaling) based on ice thickness h_{ice}, a set of dimensionless quantities are identified which describe the relative importance of physical effects, including a Reynolds number based on h_{ice} comparing the inertial to viscous force in the ice layer, and an elasticity parameter for the flexural-gravity waves in solid ice or ice layer. Through those dimensionless parameters, theories are compared. When the normalization is applied to field and lab data, scale collapse of different datasets occurs, supporting the relevance of h_{ice}. Furthermore, fitting theories to the normalized data leads to more consistent estimates of physical parameters, e.g. the effective ice viscosity and elasticity, compared to those obtained by fitting the dimensional data. The findings in Yu et al. (2019) demonstrate that appropriate scaling is important in studies of waves in ice. Most recently, Rogers et al. (2021a) analyzed the dissipation rates estimated from an extensive set of wave measurements in the Ross Sea, concluding that a positive correlation exists between k_i and h_{ice}. In their effort to improve the Navy's forecast of wind-waves in ice-infested regions, Rogers et al. (2021b) exploited this correlation invoking the scaling in Yu et al. (2019), and reported the improved prediction of k_i by appropriate inclusion of h_{ice}.

The purpose of this study, evolved from Rogers et al. (2021b), is to develop a new method for parameterizing wave dissipation that is informed by the dimensional analysis of data, and reveals not only the dependence on h_{ice} but also its relation with the dependence on frequency f. It also leads to an explicit expression of the condition of similarity, through which the apparent discrepancy between large-scale field and small-scale lab observations (as discussed above) can be resolved. The rest of the paper is as follows. Section 2 describes the dataset to be used, referring the details to Rogers et al. (2021a). In section 3, the new approach is discussed, and a new model is given and compared with other existing ones. Conclusions follow in section 4.

2 PIPERS-17 dataset

The dataset is from the wave measurements during the "Polynyas, Ice Production, and seasonal Evolution in the Ross Sea" (PIPERS) cruise in 2017 (Ackley et al., 2020). A total of 23,206 wave spectra were obtained during April-June. Details of the experiment and measurements can be found in Rogers et al. (2021a), as well as earlier publications (Kohout & Williams, 2019; Kohout et al., 2020). Applying the method of model-data inversion (Rogers et al., 2016) to 9477 wave spectra measured on 6 to 30 June, and

using WW3 as the modeling platform, Rogers et al. (2021a) estimated the wave-amplitude attenuation rates k_i. The profile $k_i(f)$ is calculated for each measured spectrum $E(f)$, then co-located with a number of additional variables, including the ice thickness $h_{\rm ice}$. However, $h_{\rm ice}$ is not used in the inversion to determine k_i. The co-location with valid contemporary estimates of $h_{\rm ice}$ reduces the data size to 8957 but does not alter the inversion outcomes. The data k_i were then classified into 16 frequency-bins over the range of 0.042 to 0.47 Hz, with the bin width increasing with f.

Ice thickness is available for the PIPERS dataset from two sources: in situ observations during instrument deployment (Kohout & Williams, 2019; Kohout et al., 2020), and remotely sensed $h_{\rm ice}$ derived from the MIRAS radiometer onboard the European Space Agency's SMOS satellite. The SMOS $h_{\rm ice}$ is capped at 50 cm, where the instrument saturates. The SMOS $h_{\rm ice}$ is a relatively new, first-generation product (Kaleschke et al., 2012; Huntemann et al., 2014), and in general not expected to have the same level of accuracy as other more mature satellite products. Since the product is intended for the "freeze-up period" (Huntemann et al., 2014), it is most suitable for sheet ice. For broken floes formed from new sheet ice (as is the case in PIPERS), it may be more appropriate to interpret $h_{\rm ice}$ as an "equivalent ice thickness".

The bin-averaged attenuation profiles $k_i(f)$ are shown in Figure 2a, and color-coded based on the associated $h_{\rm ice}$ (the co-located SMOS $h_{\rm ice}$). A striking feature is that the profiles are clearly separated for cases with $h_{\rm ice} > 14$ cm, and $k_i(f)$ is positively correlated with $h_{\rm ice}$. The trends of $k_i(f)$ are generally similar, despite being separated, though irregular variations are seen in those in thinner ice. It is also clear that the general trend of $k_i(f)$ of the PIPERS dataset is different from the binomial model $k_i = C_2 f^2 + C_4 f^4$ given by Meylan et al. (2014), which does not include the dependence on $h_{\rm ice}$. (The binomial fit is based on the SIPEX-II dataset, which has 268 data, much smaller than the PIPERS dataset.) The binomial calibrated in Rogers et al. (2018a,b) for the Arctic 'Sea State' dataset is seen to be comparable with the PIPERS data in thin ice and for $f >$ 0.1 Hz. For the 'Sea State' experiment, $h_{\rm ice}$ estimated from the frazilometer data (Wadhams et al., 2018) are mostly around 5 to 10 cm. It is evident that a parametric model is needed to describe the dependence on $h_{\rm ice}$ and its increasing influence in thicker ice, as seen in the PIPERS dataset.

3 The new approach and model $k_i(f, h_{\text{ice}})$

Following Yu et al. (2019), we define the dimensionless attenuation rate and angular frequency

$$\widehat{k_i} = k_i h_{\text{ice}}, \quad \hat{\omega} = \omega\sqrt{h_{\text{ice}}/g}, \tag{1}$$

where $\omega = 2\pi f$, and g is the gravitational acceleration. Using the co-located h_{ice} for each data point, we plot the normalized PIPERS dataset in Figure 2b, where the scale collapse of data is immediately seen. For polynomial fits in the $(\widehat{k_i}, \widehat{\omega})$ plane, $\widehat{k_i} = c_0\widehat{\omega}^0 + c_1\widehat{\omega}^1 + \cdots + c_n\widehat{\omega}^n$, and the dependence on h_{ice} follows upon returning to the dimensional form. For instance, a monomial fit $\widehat{k_i} = c_n\widehat{\omega}^n$ gives

$$k_i = c_n \left(2\pi/\sqrt{g}\right)^n h_{\text{ice}}^{n/2-1} f^n. \tag{2}$$

The collapsed data do suggest a monomial, and the best fit is $\widehat{k_i} = 0.108\widehat{\omega}^{4.46}$ (Figure 2b). On the open water (without ice), $\omega^2 = gk_{\text{ow}}$, where k_{ow} is the deep-water wavenumber. Field observations of waves in ice generally show little deviation of wavelength from its open-water value $2\pi/k_{\text{ow}}$; e.g. Collins et al. (2018) indicated only a small change in wavenumber at $f > 0.3$ Hz. Thus, we assume here that the wavenumber is k_{ow}, and rewrite (2) into

$$k_i/k_{\text{ow}} = c_n \left(k_{\text{ow}} h_{\text{ice}}\right)^{n/2-1}. \tag{3}$$

Whereas (2) is convenient for practical applications because of its direct use of f, the alternative form (3) is insightful and expresses a condition of similarity between model (lab) and prototype (field) since it involves the ratios among three lengths: the e-folding distance $1/k_i$ of wave-amplitude decay, ice thickness h_{ice} and wavelength $2\pi/k_{\text{ow}}$. As wavelength is determined by frequency f via acceleration g, (3) is not simply a condition for geometric similarity but related to dynamic similarity. Both formulae can be safely used in any system of units, as c_n is dimensionless.

This analysis not only finds the power n of f, but also reveals how the dependence on h_{ice} is related to that on f. Indeed, a purpose of dimensional analysis is to seek the relations among the physical variables that are significant to the phenomenon in question. In the dimensionless plane, the relations become more apparent due to reduced number and complexity of variables, which is manifested by the scale collapse of data as seen in Figure 2b.

Consider fitting the dimensional data in Figure 2a using a monomial

$$k_i = C h_{\rm ice}^m f^n, \tag{4}$$

assuming all data points are equally weighted. Following (2), $n = 4.46$ and $m = 1.23$. For a slight simplicity, we take $n = 4.5$, hence $m = 1.25$. Calibrating the coefficient by minimizing the magnitude of bias, we obtain

$$k_i = C h_{\rm ice}^{1.25} f^{4.5}, \text{ where } C = 0.1274\,(2\pi/\sqrt{g})^{4.5}, \tag{5}$$

or alternatively,

$$k_i/k_{\rm ow} = 0.1274\,(k_{\rm ow} h_{\rm ice})^{5/4}. \tag{6}$$

For $g = 9.83$ m/s^2 in polar regions, $C = 2.91$ (SI units) in (5). The difference between (5) and that using $n = 4.46$, $m = 1.23$ is barely visible.

A number of parametric models exist in the literature; see the review discussion in Rogers et al. (2021a,b). Early studies emphasize the dependence on f alone, e.g., the binomial form mentioned above, which has been implemented in WW3 and SWAN. For the PIPERS dataset, Rogers et al. (2021a) found that the mean, averaged over the dissipation profiles in thinner ice near the ice edge ($h_{\rm ice} < 14$ cm), can be well fitted by such a binomial, and equally well by a monomial with n from 3.5 to 4. The average, of course, removes the variability due to $h_{\rm ice}$ which in fact is very mild for $h_{\rm ice} < 14$ cm (Figure 2a). For comparison, we calibrate the monomial (including all profiles) with $m = 0$ and varying n from 3 to 4.5, and find that the fit with $n = 4$ is slightly better. We call this the case $n = 4$, $m = 0$. Meylan et al. (2018) suggested an order 3 power law with a linear dependence on $h_{\rm ice}$ by assuming a relation for the energy loss; see also Liu et al. (2020). This is the case $n = 3$, $m = 1$. Doble et al. (2015) also proposed a linear dependence on $h_{\rm ice}$ based on the data for waves of period 8 s in changing ice thickness. We find that their formula, $k_i \sim h_{\rm ice} f^{2.13}$, over-predicts k_i, often by an order of magnitude, though there is a fair agreement at higher frequencies and in thicker ice. This case is not included here, but was discussed in Rogers et al. (2021b).

The results of monomial fits are summarized in Table 1, and compared with the new model (5). The scatter index SI (the normalized standard deviation) is similar for $n = 3$, $m = 1$ (SI = 0.068) and for $n = 4$, $m = 0$ (SI = 0.063), whereas SI = 0.038 for $n = 4.5$, $m = 1.25$, meaning that scatter is reduced by 40% using the new model. This is clearly seen from the scatter plots (Figure 3). While all fittings are performed in the

dimensional plane, the new model is significantly better because the powers n and m are informed by analyzing the normalized data, and related. In fact, if we had taken $n = 4$ instead of $n = 4.5$ to approximate $n = 4.46$, we would have had $m = n/2 - 1 = 1$, a linear dependence on $h_{\rm ice}$ as in Meylan et al. (2018). However, SI = 0.041 for $n = 4$, $m = 1$, which is much lower than that for Meylan et al.'s case $n = 3$, $m = 1$, though still higher than SI = 0.038 for $n = 4.5, m = 1.25$. This indicates the significance of having the appropriate relation between the dependence on $h_{\rm ice}$ and on f. We note that in their theoretical study of a two-layer fluid system, Sutherland et al. (2019) derived $k_i \sim k_{\rm ow}^2 h_{\rm ice}$ by hypothesizing a closure for the effective ice viscosity ν (unlike other studies which generally treat ν as a given property). Since $\omega^2 = g k_{\rm ow}$, this in effect is a case of $n = 4$, $m = 1$.

Although $m = 1.25$ is not so different from $m = 1$, it renders the dependence on $h_{\rm ice}$ nonlinear, predicting an increasingly amplified influence of ice as $h_{\rm ice}$ increases. It is seen in Figure 2a that $k_i(f)$ in thicker ice are more clearly separated than those in thiner ice. This nonlinear dependence can have more implications in predicting low-frequency waves, since they can penetrate into thick ice.

The field and lab datasets in Figure 1 (except for the SIPEX-II dataset) were considered in Yu et al. (2019) for normalization using (1). Those and the PIPERS dataset are plotted together in Figure 4. The new model (5) is rewritten into $\widehat{k_i} = 0.1274\widehat{\omega}^{4.5}$ and included in Figure 4b. In view that these datasets are from independent studies, in different scales and from different polar regions, it is remarkable that they all collapse towards the new model in the dimensionless plane. A few points are worth noting: (i) While they are disconnected from the field datasets in the dimensional plane, the normalized lab datasets match well with the extrapolation of (5). Thus, a condition of similarity exist between the small-scale lab and large-scale field observations, as the alternative form (6) states. The normalized datasets of Zhao & Shen (2015) overlap with the 'Sea State' data of large $\widehat{\omega}$, meaning that those waves in the ice-covered tank are similar to the high-frequency field waves in thicker ice. (ii) In dimensional form, Doble et al.'s data are not comparable with other field datasets, but upon normalization they show some similarity with the PIPERS profiles in thicker ice (red curve), and with some 'Sea State' data. Note that the majority of Doble et al.'s datasets was in ice with estimated $h_{\rm ice} > 30$ cm. (iii) The PIPERS and lab data have better documentation of $h_{\rm ice}$, and become least scattered upon normalization. This is not a coincidence, but evidence that

$h_{\rm ice}$ is a dominant scaling in analyzing k_i. (iv) Although it has only a slightly higher SI than the new model $n = 4.5, m = 1.25$ when calibrated for the PIPERS dataset, the case $n = 4, m = 1$ is clearly more biased when other datasets are included, and significantly under-predicts the lab data; see the dotted line in Figure 4b.

In theoretical studies, other physical properties, in addition to $h_{\rm ice}$, are involved, e.g. the effective ice viscosity and elasticity. While empirical approaches based on data-fitting do not have the burden to deal with those complex physical properties, their effects still exist, meaning that we do not expect all data to collapse onto one single curve in the plane $(\widehat{k_i}, \widehat{\omega})$. In other words, the coefficient, perhaps even the exponents, of a parametric model may vary based on individual datasets, a manifestation that k_i is affected by other properties of the ice field.

4 Conclusions

We have demonstrated that the method, based on the dimensional analysis of data, can significantly improve the parameterization of wave dissipation in sea ice. The normalization (1) collapses data towards a general trend, making it evident that $h_{\rm ice}$ is an important scale when searching for similarities among data. Analyzing the PIPERS data informs a new model of form $k_i \sim h_{\rm ice}^{n/2-1} f^n$, or alternatively, $k_i/k_{\rm ow} \sim (k_{\rm ow} h_{\rm ice})^{n/2-1}$ which states a condition of similarity between data in different scales. With $n = 4.5$, it leads to a nonlinear dependence on $h_{\rm ice}$, predicting an increasingly amplified effect of ice in thicker $h_{\rm ice}$. This can have more implications in predicting low-frequency waves, since ice acts as a low-pass filter on waves. Relative to other calibrated monomials, we find that scatter is reduced by 40% using the new model (5), when applied to the PIPERS dataset. When extrapolated, (5) agrees very well with a number of lab datasets from different studies. This shows that the apparent dissimilarity between field and lab datasets in the dimensional plane, can be resolved via appropriate scaling, as the condition of similarity (6) explicitly states.

For further validation and improvement, we recommend: (i) re-analyze other existing field datasets, e.g., Meylan et al. (2014) and Doble et al. (2015), using model-data inversion, so that methods of estimating k_i are consistent; (ii) improve the estimates of $h_{\rm ice}$ by, e.g. accounting for ice concentration, and including other satellite observations such as SMAP (Soil Moisture Active Passive). For the Navy's operational modeling, we

have recommended to implement the model $k_i = Ch_{\text{ice}}^{n/2-1} f^n$ in WW3 and SWAN, with a default setting as (5).

Acknowledgments

This work is founded by the Office of Naval Research (ONR) under Program Element 61153N, and NRL 6.1 Project "Wave Propagation in Marginal Ice Zones" (PI: M. Orzech). WER is also funded by ONR (Program Manager: S. Harper) for the project "Wave-ice-ocean interaction along the Arctic Coast" (led by J. Thomson who is funded separately at Univ. Washington). This is NRL/JA-7320-21-5276 approved for public release.

Data Availability Statement:

PIPERS dissipation profiles are available from Mendeley Data, doi:10.17632/5b742jv7t5.1. Other data are available through Rogers et al. (2018a,b), Doble et al. (2015), Newyear and Martin (1997), Wang and Shen (2010), Zhao and Shen (2015), Parra et al. (2020).

References

Ackley, S.F., Stammerjohn, S., Maksym, T., Smith, M., Cassano, J., Guest, P., Tison, J.-L., Delille, B., Loose, B., Sedwick, P., DePace, L., Roach, L., & Parno, J. (2020). Sea-ice production and air/ice/ocean/ biogeochemistry interactions in the Ross Sea during the PIPERS 2017 autumn field campaign. *Ann. Glaciol.*, **61**(82), 181–195.

Booij, N., Ris, R.C. & Holthuijsen, L. H. (1999). A third-generation wave model for coastal regions, Part 1: Model description and validation. *J. Geophys. Res.*, **104**(C4), 7649-7666.

Cheng, S., Rogers, W.E., Thomson, J., Smith, M., Doble, M.J., Wadhams, P., Kohout, A.L., Lund, B., Persson, O.P.G., Collins III, C.O., Ackley, S.F., Montiel, F., & Shen, H.H. (2017). Calibrating a viscoelastic sea ice model for wave propagation in the Arctic fall marginal ice zone. *J. Geophys. Res. Oceans*, **122**, 8770-8793.

Collins, C., Doble, M., Lund, B., & Smith, M. (2018). Observations of surface wave dispersion in the marginal ice zone. *J. Geophys. Res.*, **123**, doi:10.1029/2018JC01378.

Doble, M., De Carolis, G., Meylan, M.H., Bidlot, J.-R., & Wadhams, P. (2015). Relating wave attenuation to pancake ice thickness, using field measurements

and model results. *Geophys. Res. Lett.*, **42**, 4473-4481.

Huntemann, M., Heygster, G., Kaleschke, L., Krumpen, T., Mäkynen, M., & Drusch, M. (2014). Empirical sea ice thickness retrieval during the freeze-up period from SMOS high incident angle observations. *The Cryosphere*, **8**, 439-451, doi:10.5194/tc-8-439-2014.

Kaleschke, L., Tian-Kunze, X., Maaß, N., Mäkynen, M., & Drusch, M. (2012). Sea ice thickness retrieval from SMOS brightness temperatures during the Arctic freeze-up period. *Geophys. Res. Lett.*, **39**, L05501, doi:10.1029/2012GL050916.

Kohout, A.L., Williams, M.J.M., Dean, S.M., & Meylan, M.H. (2014). Storm-induced sea-ice breakup and the implications for ice extent. *Nature*, **509**, 604–607.

Kohout, A.L., & Williams, M.J.M. (2019). Antarctic wave-ice observations during PIPERS. *NIWA client report 2019060CH prepared for the Deep South Challenge*. National Institute of Water and Atmospheric Research, New Zealand. Contact: library@niwa.co.nz.

Kohout, A.L., Smith, M., Roach, L.A., Williams, G., Montiel, F., & Williams, M.J.M. (2020). Observations of exponential wave attenuation in Antarctic sea ice during the PIPERS campaign. *Ann. Glaciol.*, **61**(82), 196-209.

Liu, Q., Rogers, W.E., Babanin, A., Li, J., & Guan, C. (2020). Spectral modeling of ice-induced wave decay. *J. Phys. Oceanogr.*, **90**, 1583–1604.

Meylan, M.H., Bennetts, L.G., & Kohout, A.L. (2014). In situ measurements and analysis of ocean waves in the Antarctic marginal ice zone. *Geophys. Res. Lett.*, **41**, 5046-5051.

Meylan, M.H., Bennetts, L.G., Mosig, J.E.M., Rogers, W.E., Doble, M.J., & Peter, M.A. (2018). Dispersion relationships, power laws, and energy loss for waves in the marginal ice zone. *J. Geophys. Res. Oceans*, **123**, 3322-3335.

Newyear, K., & Martin, S. (1997). A comparison of theory and laboratory measurements of wave propagation and attenuation in grease ice. *J. Geophys. Res.*, **102**(C11), 25091-25099.

Parra, S.M., Sree, D.K.K., Wang, D.W., Rogers, W.E., Lee, J.H., Collins III, C.O., Law, A.W., & Babanin, A.V. (2020). Experimental study on surface wave modifications by different ice covers. *Cold Reg. Sci. Technol.*, **174**, 103042.

Rogers, W.E., Thomson, J., Shen, H.H., Doble, M.J., Wadhams, P., & Cheng, S. (2016). Dissipation of wind waves by pancake and frazil ice in the autumn Beaufort Sea. *J. Geophys. Res. Oceans*, **121**, 7991-8007.

Rogers, W.E., Posey, G.P., Li, L., & Allard, R.A. (2018a). Forecasting and hindcasting waves in and near the marginal ice zone: Wave modeling and the ONR "Se State" field experiment. *NRL Memorandum Report. NRL/MR/7320-18-9786*. Naval Research Laboratory, Stennis Space Center, MS. 179pp. ww7320.nrlssc.navy.mil/pubs.php.

Rogers, W.E., Meylan, M.H., & Kohout, A.L. (2018b). Frequency distribution of dissipation of energy of ocean waves by sea ice using data from Wave Array 3 of the ONR "Sea State" field experiment. *NRL Memorandum Report. NRL/MR/7320-18-9801*. Naval Research Laboratory, Stennis Space Center, MS. 25pp. ww7320.nrlssc.navy.mil/pubs.php.

Rogers, W.E. (2020). Phase-averaged wave models. In *Ocean Wave Dynamics*, Young, I. and Babanin, A. eds., 163-204. World Scientific.

Rogers, W.E., Meylan, M.H., & Kohout, A.L. (2021a). Estimates of spectral wave attenuation in Antarctic sea ice, using model/data inversion. *Cold Reg. Sci. Technol.*, **182**, 103198.

Rogers, W.E., Yu, J., & Wang, D.W. (2021b). Incorporating dependence on ice thickness in empirical parameterizations of wave dissipation by sea ice. *NRL Technical Report. NRL/OT/7320-21-5145*. Naval Research Laboratory, Stennis Space Center, MS. 35pp. ww7320.nrlssc.navy.mil/pubs.php.

Sutherland, G., Rabault, J., Christensen, K.H., & Jensen, A. (2019). A two layer model for wave dissipation in sea ice. *Appl. Ocean Res.*, **88**, 111-118.

SWAN team (2019). SWAN User Manual, SWAN Cycle III version 41.31. Delft University of Technology, http://www.swan.tudelft.nl, 135 pp.

Tolman, H.L. (1991). A Third-generation model for wind-waves on slowly varying, unsteady, and inhomogeneous depths and currents. *J. Phys. Oceanogr.*, **21**(6), 782-797.

Wadhams, P., Aulicino, G., Parmiggiani, F., Persson, P.O.G., & Holt, B. (2018). Pancake ice thickness mapping in the Beaufort Sea from wave dispersion observed in SAR imagery. *J. Geophys. Res. Oceans*, **123**, 2213-2237.

Wang, R., & Shen, H.H. (2010). Experimental study on surface wave propagating

through a grease-pancake ice mixture. *Cold Reg. Sci. Technol.*, **61**, 90-96.

The WAVEWATCH III®Development Group (2019). User manual and system documentation of WAVEWATCH III version 6.07. *Tech. Note* **333**, NOAA/NWS/NCEP/MMAB, College Park, MD, USA, 465 pp. + Appendices.

Zhao, X., & Shen, H.H. (2015). Wave propagating in frazil/pancake, pancake, and fragmented ice covers. *Cold Reg. Sci. Technol.*, **113**, 71-80.

Yu, J., Rogers, W.E., & Wang, D.W. (2019). A scaling for wave dispersion relationships in ice-covered waters. *J. Geophys. Res. Oceans*, **124**. Doi: 10.1029/2018JC014870

Table 1. Best fits of monomial in the form of $k_i = Ch_{\rm ice}^m f^n$ (in SI units). RMSE = root-mean-square error, CC = Pearson correlation coefficient, STDD = standard deviation, and scatter index SI = STDD/mean, where mean = 5.009 is the magnitude of average $\langle \log_{10} k_{i,obs} \rangle$.

C	m	n	RMSE	CC	STDD	SI
0.094	0	4	0.312	0.924	0.315	0.063
0.059	1	3	0.337	0.967	0.340	0.068
0.59	1	4	0.205	0.974	0.207	0.041
2.91	1.25	4.5	0.186	0.973	0.188	0.038

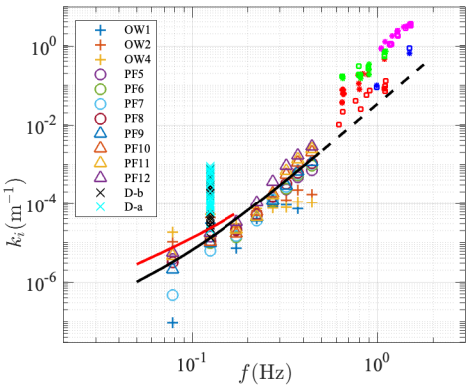

Figure 1. Field and lab datasets (k_i, f). In the legend: OW1-PF12, Arctic 'Sea State' dataset with 11 classifications indicating visually observed $h_{\rm ice}$ (Yu et al., 2019); ×, two datasets (at $f = 1/8$ Hz) in Doble et al. (2015; their figure 2). Curves: red, fit for the Antarctic SIPEX-II dataset (not shown) in Meylan et al. (2014); black, fit for the 'Sea State' data in Rogers et al. (2018a,b), with its extrapolation shown as the dashed curve. The smaller symbols (not in the legend) above the field data are from lab studies with documented $h_{\rm ice}$: magenta, two tests in Newyear & Martin (1997); green, two tests in Wang & Shen (2010); red, three tests in Zhao & Shen (2015); blue, Parra et al. (2020).

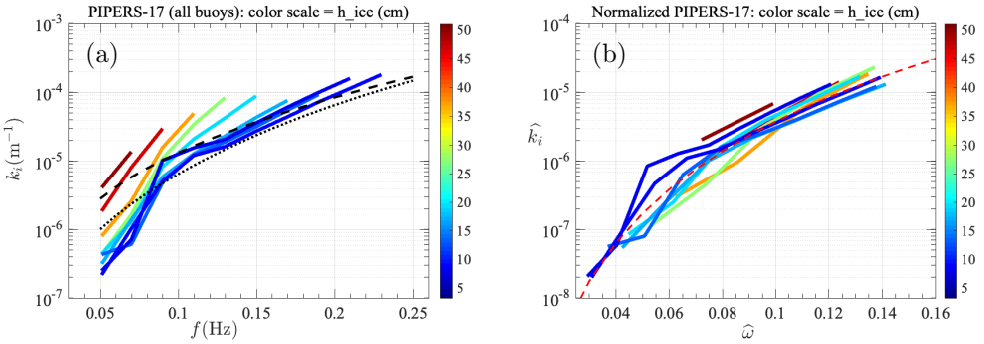

Figure 2. (a) PIPERS dataset $k_i(f)$, color-coded based on the associated h_{ice}. The data correspond to that in figure 6a in Rogers et al. (2021a). Binomial model $k_i = C_2 f^2 + C_4 f^4$: dashed, C_2, C_4 = 1.06-3, 2.30e-2 in Meylan et al. (2014); dotted, C_2, C_4 = 3.21e-4, 3.26e-2 in Rogers et al. (2018a,b). (b) Normalized PIPERS dataset. Dashed red: $\widehat{k}_i = 0.108\widehat{\omega}^{4.46}$.

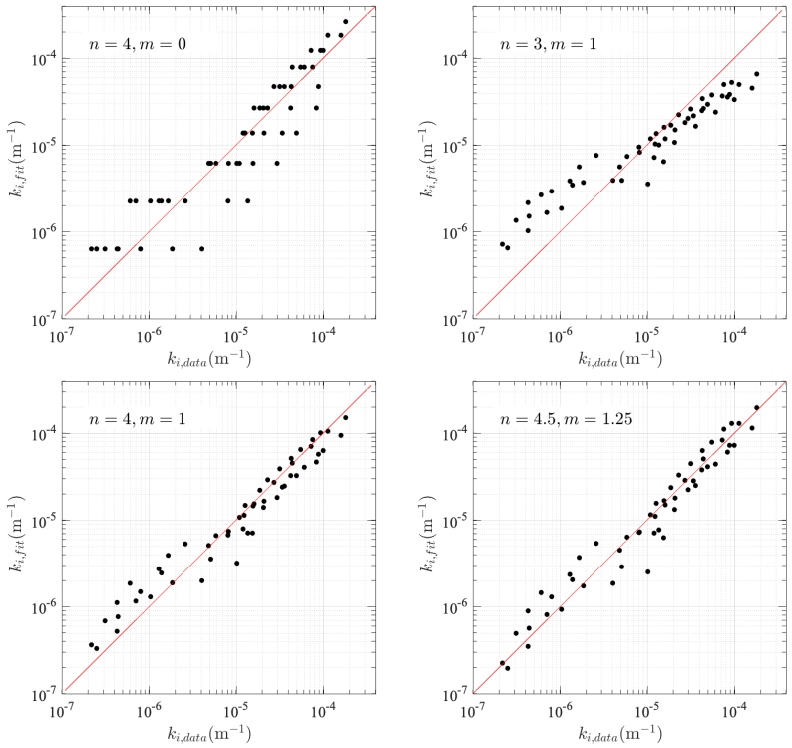

Figure 3. Scatter plots, comparing the monomial fit against the PIPERS data.

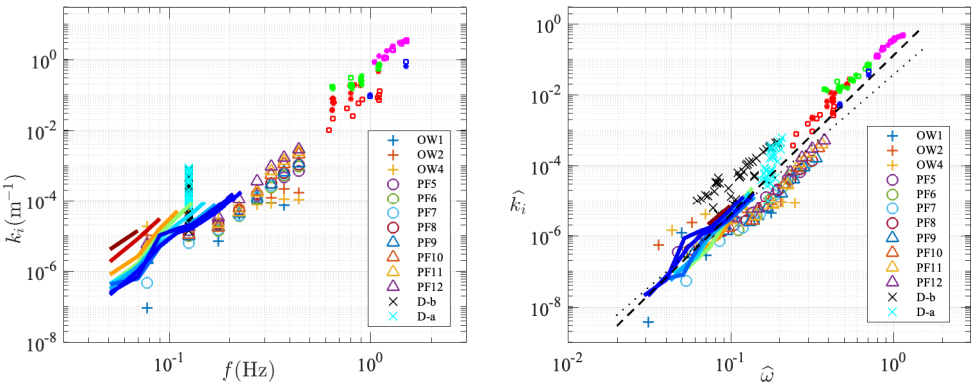

Figure 4. (a) Dimensional plot of the PIPERS dataset (thick solid), and the field and lab datasets (symbols) from Figure 1. (b) Normalized datasets; see Yu et al. (2019) for h_{ice} associated with the datasets from Figure 1. Dashed: $\widehat{k_i} = 0.1274\widehat{\omega}^{4.5}$ (new model $n = 4.5, m = 1.25$). Dotted: $\widehat{k_i} = 0.0366\widehat{\omega}^4$ (case $n = 4, m = 1$).